Giant magnetic anisotropy energy and long coherence time of uranium substitution on defected Al$_2$O$_3$(0001)

Jie Li [●], Lei Gu, and Ruqian Wu [●][*]

Department of Physics and Astronomy, University of California, Irvine, California 92697-4575, USA

Nanomagnets with giant magnetic anisotropy energy and long coherence time are desired for various technological innovations such as quantum information procession and storage. Based on the first-principles calculations and model analyses, we demonstrate that a single uranium atom substituting Al on the Al$_2$O$_3$(0001) surface may have high structural stability and large magnetic anisotropy energy up to 48 meV per uranium atom. As the magnetization resides in the localized f shell and is not much involved in chemical bonding with neighbors, long coherence time up to $\sim$1.6 mS can be achieved for the quantum spin states. These results suggest a different strategy for the search of ultrasmall magnetic units for diverse applications in the quantum information era.

I. INTRODUCTION

As potential building blocks for quantum computing [1–3] and data storage [4,5] devices, nanomagnets and molecular magnets have received increasing attention in recent years. Exceedingly large magnetic anisotropy energy (MAE) is typically required to combat thermal fluctuation and to set appropriate energy levels for quantum operations. However, MAEs of most nanomagnets are only a few tenth millielectronvolts (meV), that vitally inhibits their exploitation. Therefore, it is desired to search for new magnetic systems with large MAEs and, furthermore, long coherence time of their quantum spin states. So far, several systems were reported to have MAE > 30 meV, such as freestanding and supported transition metal dimers [6–9] or single transition metal adatoms on CuN, Rh, and MgO(100) surfaces [10–13]. It is recognized that one needs to place magnetic atoms with strong spin-orbit coupling (SOC) in an environment with weak crystal field for attaining large MAE. Furthermore, the reduction of the spin-vibration coupling is another important issue for magnetic units being used in quantum information devices.

Rare-earth and actinide atoms have unique advantages as their magnetism stems from the localized f shells, which are protected by the $s, p,$ and d outer shells and are not much involved in chemical bonds with their neighbors in compounds or alloys. Molecular magnets with rare-earth and actinide ingredients have been extensively investigated in different research fields such as for manipulating of nuclear spins [14,15], attaining quantized spin states [16], and achieving atomic clock transitions for robust qubits [3]. With strong SOC and small crystal-field splitting, the behavior of f electrons is not much different from that in isolated atoms, i.e., with large orbital moments and quantized energy levels with j being a good quantum number. As their magnetic features are not directly related to chemical bonding with neighbors, the spin-vibration coupling is expected to be weak, suitable for getting long coherence time of entangled quantum spin states. Ideally, systems with rare-earth and actinide magnetic atoms may become promising candidates for quantum information processing and storage purposes.

In this work, we investigate the electronic and magnetic properties of a single uranium atom as a substituent on the Al$_2$O$_3$(0001) surface (U/Al$_2$O$_3$) through density functional theory (DFT) calculations and electrostatic model analyses. The similar trivalent characteristics between uranium and aluminum atoms ensure the least disturbance to the local electronic balance and the insulating state of the film. This system is found to have a magnetic anisotropy energy as large as 48 meV per U atom and a long relaxation time (1.6 mS) at a reasonably high temperature (10 K), which may offer strong thermal stability as needed for practical use. Results of vibrational spectra and diffusion energies also suggest the high structural stability. This research suggests a different strategy for the design of emergent quantum materials.

II. METHODOLOGY

As depicted in Fig. 1, a 2 × 2 supercell in the lateral plane, with 18 layers of atoms and a vacuum 15 Å thick along the surface normal, was used to mimic the periodic sapphire Al$_2$O$_3$(0001) surface. The lattice constant in the lateral plane was fixed according to the experimental value of the bulk α-Al$_2$O$_3$ ($a = b = 4.76$ Å). Aluminum atoms in two surface layers were substituted by uranium atoms to keep the inversion symmetry for the computational convenience. This corresponds to a surface density of uranium substitution at 1.27×10^{18} m^{-2}. DFT calculations were carried out using the Vienna *ab initio* simulation package (VASP), at the level of the spin-polarized generalized-gradient approximation (GGA) with the functional developed by Perdew-Burke-Ernzerhof

_____

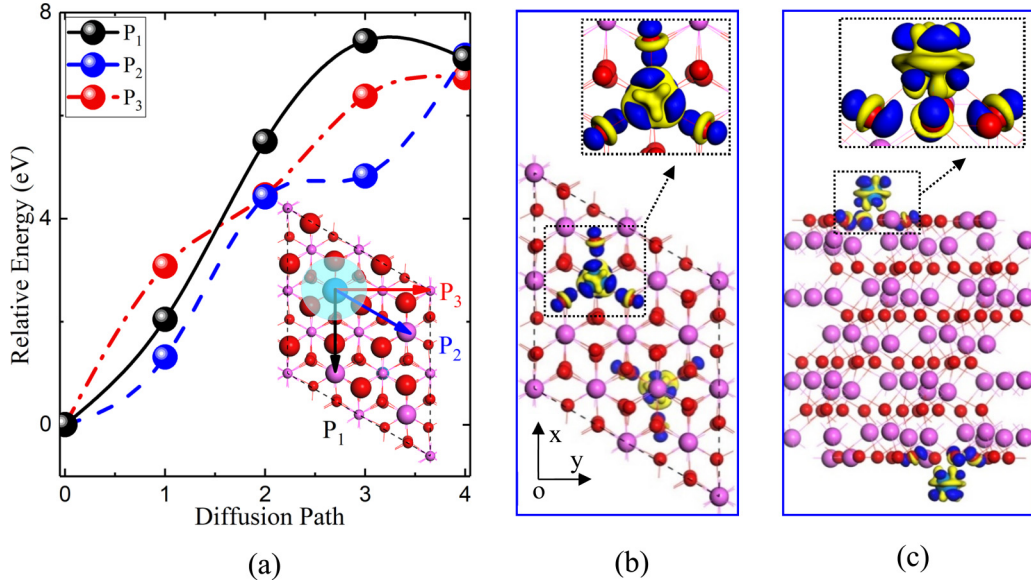*Author to whom correspondence should be addressed: wur@uci.edu

FIG. 1. (a) Three diffusion pathways of uranium atom (inset) and corresponding energy profiles. Red and pink spheres represent O and Al atoms, respectively. To make the surface O and Al atoms more distinguishable, they are represented by larger spheres. The arrows represent the diffusion pathways for energy calculations. (b), (c) The top and side views of charge density difference, i.e., $\rho(\text{U/Al}_2\text{O}_3) - \rho(\text{Al}_2\text{O}_3) - \rho(\text{U})$. Blue and yellow colors represent charge accumulation and depletion, respectively.

(PBE) [17]. Hubbard U was adopted to describe the electron correlation for the f electrons of uranium, with typical values of $U = 4.50$ eV and $J = 0.54$ eV [18]. The interaction between valence electrons and ionic cores was considered within the framework of the projector augmented wave (PAW) method [19,20]. The energy cutoff for the plane-wave basis expansion was set to 500 eV. To sample the two-dimensional Brillouin zone, we used a Gamma-centered 8×8 k-grid mesh. All atoms were fully relaxed using the conjugated gradient method for the energy minimization until the force on each atom became smaller than 0.01 eV/Å, and the energy convergence in all DFT calculations in this work was better than 10^{-8} eV.

III. RESULTS AND DISCUSSION

We first determined the binding energies of uranium atoms according to

$$\Delta E_{\text{U/Al}_2\text{O}_3} = E_{\text{Al}_2\text{O}_3} + \mu_\text{U} - E_{\text{U/Al}_2\text{O}_3} \qquad (1)$$

where $E_{\text{Al}_2\text{O}_3}$ and $E_{\text{U/Al}_2\text{O}_3}$ represent the total energies of the defected $\text{Al}_2\text{O}_3(0001)$ surface without and with uranium taking the vacancy site, respectively. μ_U is the chemical potential of a uranium atom which was set to be equal to the energy per atom in a uranium dimer. After the removal of the topmost Al atoms, uranium takes the Al-vacancy (Al_V) site with a huge energy gain, up to $\Delta E_{\text{U/Al}_2\text{O}_3} = 14.9$ eV. This is even larger than the corresponding binding energy of Al atom (12.1 eV) and clearly indicates that uranium atoms are strongly anchored to the defected $\text{Al}_2\text{O}_3(0001)$ surface. As the uranium atom has a bigger size than the aluminum atom, it shifts out of the surface plane by 1.24 Å and the bond length between uranium and the nearest three oxygen atoms is 2.14 Å.

We further considered the structural stability of $\text{U/Al}_2\text{O}_3$ against sideways displacements of uranium along pathways

depicted as P_1, P_2, and P_3 in Fig. 1(a). While doing so, we fixed the (x, y) coordinates of the uranium atom along the pathways and allowed all other atoms as well as the z coordinate of the uranium atom to fully relax. From the relative energies of diffusion, one may see that the uranium atom is tightly anchored at the Al_V site, with rapid increases of energy as it drifts away along all three pathways. In other words, uranium atoms may quickly segregate to the substitutional sites on the $\text{Al}_2\text{O}_3(0001)$ surface in experiments since the binding energy for them at the Al_V site is significantly lower than those on the flat regions, which offers a large possibility to deposit single uranium atoms on the defected $\text{Al}_2\text{O}_3(0001)$ surface.

Each trivalent uranium atom donates three electrons to its oxygen neighbors, as shown by the charge-density difference in Figs. 1(b) and 1(c). The charge transfer is limited to the surface layer, and a slight surface reconstruction occurs. The band structure of $\text{U/Al}_2\text{O}_3$ in Fig. 2(a) shows that the s and d bands of uranium are empty, and three flat f bands of uranium are occupied in the wide band gap of $\text{Al}_2\text{O}_3(0001)$. This is ideal as we seek for the separation of sources of chemical bonding (the outer s and d electrons) and magnetization (the localized f electrons). Furthermore, the insulating state with large band gap is beneficial for resisting surface oxidation and minimizing the coupling between spin and electron excitations. The calculated spin magnetic moment of each uranium atom is $\sim 3\,\mu_\text{B}$, accompanied by small negative magnetic moments of $\sim 0.09\,\mu_\text{B}$ from three neighboring O atoms. Due to the strong localization and spin-orbit coupling in the f shell, each uranium atom also has a large orbital magnetic moment up to $3.2\,\mu_\text{B}$ antiparallel to the spin moment, very different from cases with transition metal magnetic atoms for which the orbital magnetic moments are mostly quenched.

The U atom embedded in $\text{Al}_2\text{O}_3(0001)$ has a C_{3v} local symmetry and the standard spin Hamiltonian describing the
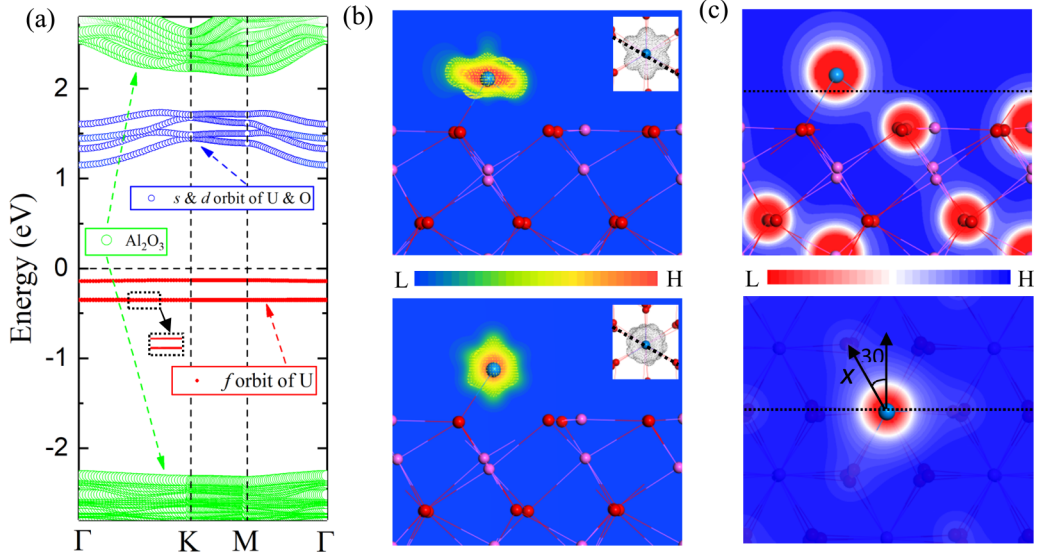
FIG. 2. (a) The band structure of U/Al_2O_3. (b) Charge density of f electrons of U/Al_2O_3 with the magnetization axis pointing along the normal and in-plane direction, respectively. (c) Side and top views of electrostatic potential of Al/Al_2O_3 with Al atoms at the U site.

single-ion anisotropy can be written as

$$H_{spin} = D_{xx}S_x^2 + D_{yy}S_y^2 + D_{zz}S_z^2 + D_{xy}(S_xS_y + S_yS_x)$$
$$+ D_{xz}(S_xS_z + S_zS_x) + D_{yz}(S_yS_z + S_zS_y), \quad (2)$$

where the D tensor represents the single-ion magnetic anisotropy parameters as we view spin as a vector. According to the four states mapping method [21], we calculated total energies of different spin configurations with the SOC term in the self-consistence (details are shown in the Supplemental Material [22]). By fitting these energies, the D tensors are obtained, as shown in Table SI of the Supplemental Material [22]. In particular, the perpendicular and in-plane magnetic anisotropy energies are given by $D_{xx}S_x^2 - D_{zz}S_z^2$ (-48.1 meV) and $D_{xx}S_x^2 - D_{yy}S_y^2$ (-26.0 meV), which indicate that this system has an in-plane easy axis along the x direction. Large anisotropy energy barriers for the magnetic moment rotating toward both y and z axes suggest that the magnetization is strongly pinned along the x axis at a reasonably high temperature. To ensure the reliability of these MAEs, test calculations with denser k-point meshes (from 16 to 100 points in the Brillouin zone) and different values of Hubbard U (0–6 eV) were done (see Figs. S1 and S2 in the Supplemental Material [22]). All results show that MAEs are converged in the present calculations.

To understand the mechanism of the giant MAEs of U/Al_2O_3, we used a simple electrostatic model which has been applied for analyzing the preferential direction of magnetization in f-electron materials [16,23]. The angle dependent energies in Eq. (2) can be estimated from the local crystal field $V_{CF}(\theta, \varphi)$ and the Sievers charge density of the uranium atom $\rho_{(\theta_S,\varphi_S)}(\theta, \varphi)$,

$$E(\theta_S, \varphi_S) = \int_{\theta=0}^{\pi} \int_{\varphi=0}^{2\pi} V_{CF}(\theta, \varphi)\rho_{(\theta_S,\varphi_S)}(\theta, \varphi) \sin(\theta)d\theta d\varphi.$$
$$(3)$$

Here, $\rho_{(\theta_S,\varphi_S)}(\theta, \varphi)$ is the charge density of f electrons that follows the spin orientation (θ_S, φ_S) as depicted in Fig. 2(b),

and $V_{CF}(\theta, \varphi)$ is extracted from the electrostatic potential which includes the ionic, Hartree, and exchange correlation parts as shown in Fig. 2(c). For $U/Al_2O_3(0001)$, three oxygen anions have the most important influence on the uranium atom and $V_{CF}(\theta, \varphi)$ has a C_{3v} symmetry. Considering the two possible orientations of the easy axis, i.e., normal (the z axis) and in-plane directions (the x axis), we plotted the corresponding charge densities of the f electrons of uranium in Fig. 2(b). One may see that the distribution pattern of $5f$ electrons somewhat follows the rotation of magnetization. Because $5f$ orbitals are rather large, we may divide them into two parts, i.e., localized part within a small sphere that rotates with spin moment due to the strong SOC, and spilled out part a distance away from uranium nuclei that are controlled by the crystal field [24]. The overall spatial distribution of $5f$ electrons of uranium is more complicated than either $4f$ electrons of rare-earth atoms or $3d$ electrons of transition metal atoms [25]. When the spin moment is set along the z axis, the f electrons of uranium form a bowl-shaped distribution as shown at the top of Fig. 2(b). Although m is no longer a good quantum number under the influence of the crystal potential, we see that $m = \pm 3$ components are well separated from others as seen from the m-projected density of states in Fig. 3(a) as the spin is align along the z axis; the case $\rho_{(\theta_S,\varphi_S)}(\theta, \varphi)$ also has the C_{3v} symmetry. Nevertheless, the weight in $m = -3$ is much larger than that in $m = +3$, showing the orbital magnetization. As the lowest nonspherical term in the crystal field is $Y_{3,\pm 3}$, $m = \pm 2$ and $m = \pm 1$ parts are degenerated. When the spin turns to the x axis, the symmetry of $\rho_{(\theta_S,\varphi_S)}(\theta, \varphi)$ is lowered. All m components intermix as we projected the f orbitals to spherical harmonics with a local "z" axis [actually the x axis as shown in the inset of Fig. 3(b)] following the rotation of spin. As the lobes of f orbitals point toward O atoms, some $Y_{3,-3}$ and $Y_{3,\pm 1}$ electrons transfer to $Y_{3,3}$ and $Y_{3,0}$ due to the influence of the crystal field, and the spatial distribution for f electrons is more isotropic as shown at the bottom of Fig. 2(b). This is also reflected in the PDOS of f orbits of the uranium atom in Fig. 3(b): three f electrons almost evenly distribute
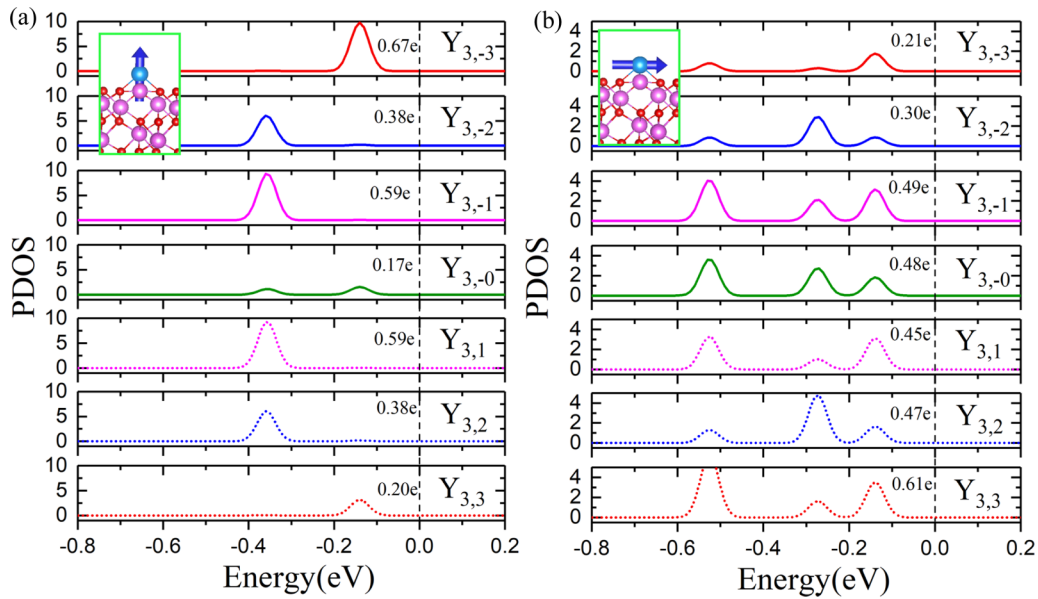
FIG. 3. (a) and (b) The projected density of states (PDOS) of f orbitals of uranium atom with the quantization axis along normal direction and in the plane, respectively.

in seven f orbits. It is obvious that the electric potential in Fig. 2(c) has significant nonspherical components around the Al or Al$_V$ site. The large MAE of U/Al$_2$O$_3$ is not only directly from SOC as for most transition metals, the crystal field also contributes due to the significant redistribution of f electrons during spin reorientation.

From the viewpoint of quantum computing, it is very important to have the magnetic sources being protected against the lattice vibration which plays an important role in magnetic fluctuation and magnonic dissipation. To this end, we explore the spin-vibration coupling (SVC) as shown in Fig. 4. From our DFT calculations, the effect of spin reorientation on the

phonon spectrum is small but obviously visible, especially for the low-frequency bands that come from the motion of uranium atom. It appears that vibrations shift to lower frequency when spin aligns in the lateral plan as shown in Fig. 4(a). For example, vibration energies of three uranium modes at the Γ point (7.14, 9.29, and 11.77 meV) shift by -0.08, 0.51, and 0.26 meV as we rotate spin from the x to z axis. As a step to estimate the SVC strength, we explored the effect of these vibrations on MAE by displacing the uranium (0.2 Å) and surrounding O and Al atoms according to the displacement vectors of these normal modes shown in the Fig. 4(a). The corresponding MAEs are 50.8, 57.5, and 88.7 (75.5, 57.5,
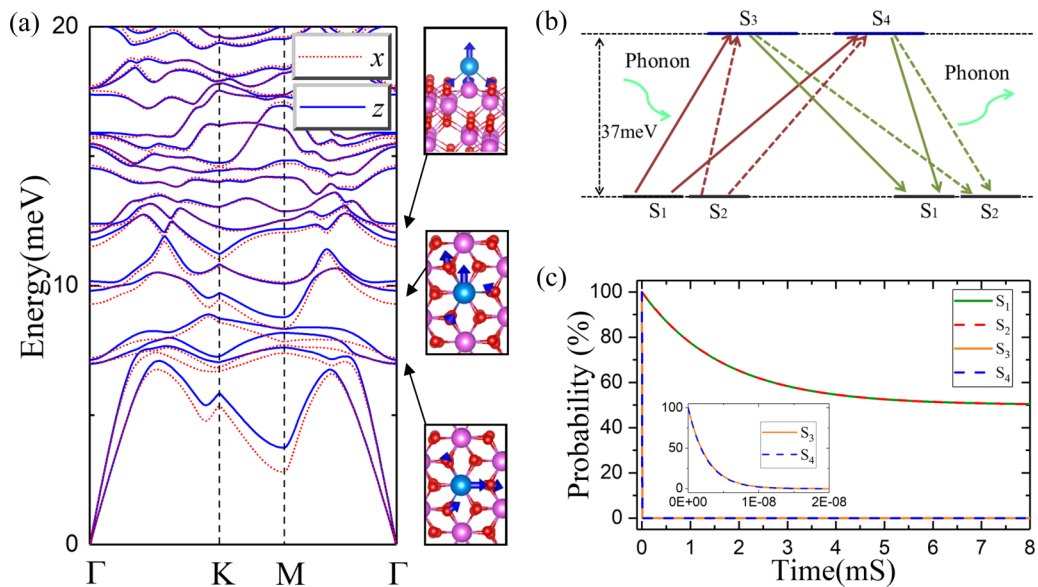

FIG. 4. (a) The phonon spectrums of U/Al$_2$O$_3$ and the schematic moving of uranium atom and three nearest oxygen atoms in three vibration models (high lines) which mostly come from the contributions of uranium atom. (b) The schematic magnetic relaxation pathways of spin states. (c) The decaying of spin states with time.

and 67.1) meV for the case of uranium atoms moving along (reverse along) the three vibrational vectors, respectively. The mutual influence between vibration and spin reorientation of uranium suggests strong SVC in this system and hence the energy exchange across the two excitations is still a concern for the system hosting quantum information.

As the D tensors are computed from energies (E_i) of four different spin configurations as

$$D_{ij} = \frac{1}{4S^2}(E_1 + E_4 - E_2 - E_3) \qquad (4)$$

we may further obtain the spin-vibration coupling coefficients by taking the derivatives of E_i with respect to u_{ka} (the displacements of atom k along the a direction), i.e.,

$$\frac{\partial D_{ij}}{\partial u_{ka}} = \frac{1}{4S^2}\left(\frac{\partial E_1}{\partial u_{ka}} + \frac{\partial E_4}{\partial u_{ka}} - \frac{\partial E_2}{\partial u_{ka}} - \frac{\partial E_3}{\partial u_{ka}}\right). \qquad (5)$$

Here, $-\frac{\partial E_i}{\partial u_{ka}}$ ($i = 1, \ldots, 4$) is the force acting on the atom k along the a direction, which can be connected to the Hellmann-Feynman force in DFT schemes with the plane-wave bases. In this work, we considered motions of the uranium atom and its three O neighbors. To find the quantum spin levels of U/Al$_2$O$_3$ (a spin 3/2 system), we recast 4 × 4 spin matrices for $S_{x,y,z}$ in Eq. (2). Using DFT parameters, there are four quantum spin states or two Kramers doublets for U/Al$_2$O$_3$ as shown in Fig. 4(b). Due to the time-reversal symmetry, phonon induced transition within each doublet is forbidden [26]. Therefore, the magnetic relaxation pathways for a ground state are those illustrated in Fig. 4(b), (details as shown in the Supplemental Material [22]). The corresponding relaxation times of these quantum spin states were calculated by using the nonequilibrium Green's-function method and the master equation. Following as Markov dynamics, the evolution of the system can be described by

$$\frac{d}{dt}p_{S_i}(t) = \sum_{S_j}\left[\gamma_{S_j}^{S_i}p_{S_j}(t) - \gamma_{S_i}^{S_j}p_{S_i}(t)\right], \qquad (6)$$

where p_{S_i} and $\gamma_{S_j}^{S_i}$ represent the probability of being at spin state S_i and the transition rate from spin state S_j to spin state S_i, respectively. As the energy barrier of the spin states is accessible to the phonon bath (0–120 meV, as shown in Fig. S3 in the Supplemental Material [22]) in this work, we only considered the relaxation caused by the first-order spin-phonon coupling, i.e., single phonon mode. Then, the transition rate from spin state S_i to spin state S_j is given by

$$\gamma_{S_i}^{S_j} = \sum_q \frac{i}{\hbar}G_q^<(\omega)|a_q|^2 \qquad \text{and}$$

$$G_q^<(\omega) = -\frac{i\pi}{\omega_q}\{\delta(\omega - \omega_q)N(\omega_q) + \delta(\omega + \omega_q)[N(\omega_q) + 1]\},$$
$$(7)$$

where $G_q^<(\omega)$ is the lesser Green's function for phonon q, and a_q is the transition matrix element of SVC, $a_q = \langle S_i|\frac{\partial H_{\text{spin}}}{\partial V_q}|S_j\rangle$ with V_q representing the atomic displacements corresponding to phonon mode q [27] (the detailed calculations are shown in the Supplemental Material [22]). By substituting

$$p_{S_j}(t) = \sum_k \varphi_{S_j}^{(k)}\exp(-t/\tau_k) \qquad (8)$$

into Eq. (6), we have

$$-\frac{1}{\tau_k}\varphi_{S_j}^{(k)} = \sum_{S_i}\left[\gamma_{S_i}^{S_j}\varphi_{S_i}^{(k)} - \gamma_{S_j}^{S_i}\varphi_{S_j}^{(k)}\right]$$
$$= \sum_{S_i}\left[\gamma_{S_i}^{S_j} - \delta_{S_i}^{S_j}\sum_{S_l}\gamma_{S_l}^{S_i}\right]\varphi_{S_i}^{(k)}. \qquad (9)$$

Therefore, eigenvalues of the coefficient matrix

$$\Gamma_{S_i}^{S_j} = \gamma_{S_i}^{S_j} - \delta_{S_i}^{S_j}\sum_{S_l}\gamma_{S_l}^{S_i} \qquad (10)$$

give the time scales. There is a zero value corresponding to the statistic state, and the smallest nonzero value characterizes the relaxation of magnetization [28]. The probabilities of holding in these spin states through relaxation are shown in Fig. 4(c). While the excited doublet quickly decays (within nS as shown in the inset), the ground states decay rather slowly, due to the high-energy barrier raised by the magnetic anisotropy. We may see from Fig. 4(c) a long coherence time (1.6 mS) at a reasonably high temperature (10 K) for the S_1 and S_2 states. This implies that U/Al$_2$O$_3$ can be a potential candidate for being developed as a quantum material.

In end, we also suggest that if the substituents are changed to rare-earth atoms, such as praseodymium and erbium atoms, the corresponding MAE can be even higher than uranium. As the SVC in a rare-earth system is much weaker than uranium as well, longer relaxation time can be expected, which may deserve experimental and theoretical explorations in the future.

IV. CONCLUSION

In summary, we investigated the structural and electronic properties of a single uranium atom as a substituent on the Al$_2$O$_3$(0001) surface. The large binding energy and high diffusion energy barriers suggest that the uranium atoms are strongly anchored to the substitutional sites. The MAE of this spin 3/2 system is as large as 48 meV and the relaxation time is up to ∼1.6 mS at 10 K. Thus, we recommend this system or similar structures with rare-earth substituents as a class of potential candidates for developing materials for quantum information processing and storage.

[1] M. N. Leuenberger and D. Loss, Quantum computing in molecular magnets, Nature (London) **410**, 789 (2001).

[2] G. Aromi, D. Aguila, P. Gamez, F. Luis, and O. Roubeau, Design of magnetic coordination complexes for quantum computing, Chem. Soc. Rev. **41**, 537 (2012).

[3] M. Shiddiq, D. Komijani, Y. Duan, A. Gaita-Arino, E. Coronado, and S. Hill, Enhancing coherence in molecular spin qubits via atomic clock transitions, Nature (London) **531**, 348 (2016).

[4] F. Donati, S. Rusponi, S. Stepanow, C. Wäckerlin, A. Singha, L. Persichetti, R. Baltic, K. Diller, F. Patthey, E. Fernandes, J. Dreiser, Z. Sljivancanin, K. Kummer, C. Nistor, P. Gambardella, and H. Brune, Magnetic remanence in single atoms, Science **352**, 318 (2016).

[5] F. D. Natterer, K. Yang, W. Paul, P. Willke, T. Choi, T. Greber, A. J. Heinrich, and C. P. Lutz, Reading and writing single-atom magnets, Nature (London) **543**, 226 (2017).

[6] T. O. Strandberg, C. M. Canali, and A. H. Macdonald, Transition-metal dimers and physical limits on magnetic anisotropy, Nat. Mater. **6**, 648 (2007).

[7] R. J. Xiao, D. Fritsch, M. D. Kuz'min, K. Koepernik, H. Eschrig, M. Richter, K. Vietze, and G. Seifert, Co Dimers on Hexagonal Carbon Rings Proposed as Subnanometer Magnetic Storage Bits, Phys. Rev. Lett. **103**, 187201 (2009).

[8] J. Hu and R. Wu, Giant magnetic anisotropy of transition-metal dimers on defected graphene, Nano Lett. **14**, 1853 (2014).

[9] J. Li, H. Wang, J. Hu, and R. Wu, Search for giant magnetic anisotropy in transition-metal dimers on defected hexagonal boron nitride sheet, J. Chem. Phys. **144**, 204704 (2016).

[10] C. F. Hirjibehedin, C. Y. Lin, A. F. Otte, M. Ternes, C. P. Lutz, B. A. Jones, and A. J. Heinrich, Large magnetic anisotropy of a single atomic spin embedded in a surface molecular network, Science **317**, 1199 (2007).

[11] P. Blonski, A. Lehnert, S. Dennler, S. Rusponi, M. Etzkorn, G. Moulas, P. Bencok, P. Gambardella, H. Brune, and J. Hafner, Magnetocrystalline anisotropy energy of Co and Fe adatoms on the (111) surfaces of Pd and Rh, Phys. Rev. B **81**, 104426 (2010).

[12] I. G. Rau, S. Baumann, S. Rusponi, F. Donati, S. Stepanow, L. Gragnaniello, J. Dreiser, C. Piamonteze, F. Nolting, S. Gangopadhyay, O. R. Albertini, R. M. Macfarlane, C. P. Lutz, B. A. Jones, P. Gambardella, A. J. Heinrich, and H. Brune, Reaching the magnetic anisotropy limit of a 3d metal atom, Science **344**, 988 (2014).

[13] X. Ou, H. Wang, F. Fan, Z. Li, and H. Wu, Giant Magnetic Anisotropy of Co, Ru, and Os Adatoms on MgO (001) Surface, Phys. Rev. Lett. **115**, 257201 (2015).

[14] R. Vincent, S. Klyatskaya, M. Ruben, W. Wernsdorfer, and F. Balestro, Electronic read-out of a single nuclear spin using a molecular spin transistor, Nature (London) **488**, 357 (2012).

[15] S. Thiele, F. Balestro, R. Ballou, S. Klyatskaya, M. Ruben, and W. Wernsdorfer, Electrically driven nuclear spin resonance in single-molecule magnets, Science **344**, 1135 (2014).

[16] C. Goodwin, F. Ortu, D. Reta, N. Chilton, and D. Mills, Molecular magnetic hysteresis at 60 kelvin in dysprosocenium, Nature (London) **548**, 439 (2017).

[17] J. P. Perdew, K. Burke, and M. Ernzerhof, Generalized Gradient Approximation Made Simple, Phys. Rev. Lett. **77**, 3865 (1996).

[18] B. Dorado, B. Amadon, M. Freyss, and M. Bertolus, DFT+U calculations of the ground state and metastable states of uranium dioxide, Phys. Rev. B **79**, 235125 (2009).

[19] P. E. Blochl, Projector augmented-wave method, Phys. Rev. B **50**, 17953 (1994).

[20] G. Kresse and D. Joubert, From ultrasoft pseudopotentials to the projector augmented-wave method, Phys. Rev. B **59**, 1758 (1999).

[21] H. Xiang, C. Lee, H. Koo, X. Gong, and M. Whangbo, Magnetic properties and energy-mapping analysis, Dalton Trans. **42**, 823 (2013).

[22] See Supplemental Material at http://link.aps.org/supplemental/10.1103/PhysRevB.102.054406 for D tensors, test calculations of MAEs with different denser k-point meshes and Hubbard U, phonon spectrums, and spin-vibration coupling.

[23] N. Chilton, D. Collison, E. Mclnnes, R. Winpenny, and A. Soncini, An electrostatic model for the determination of magnetic anisotropy in dysprosium complexes, Nat. Commun. **4**, 2551 (2013).

[24] Q. G. Sheng and B. R. Cooper, Prediction of pressure-induced changes in magnetic ordering of correlated-electron uranium systems, J. Appl. Phys. **75**, 7035 (1994).

[25] G. H. Lander, P. J. Brown, M. R. Spirlet, J. Rebizant, B. Kanellakopulos, and R. Klenze, Study of electron wave functions in uranium tetrachloride by neutron scattering, J. Chem. Phys. **83**, 5988 (1985).

[26] J. H. Van Vleck, Paramagnetic relaxation times for titannium and chrome alum, Phys. Rev. **57**, 426 (1940).

[27] A. Lunghi and S. Sanvito, How do phonons relax molecular spins? Sci. Adv. **5**, eaax7163 (2019).

[28] D. Gatteschi, R. Sessoli, and J. Villain, *Molecular Nanomagnets* (Oxford University Press, New York, 2011).